ADVANCED MATERIALS
www.advmat.de

A New Class of Cluster–Matrix Nanocomposite Made of Fully Miscible Components

Gleb Iankevich, Abhishek Sarkar, Shyam Katnagallu, Mohammed Reda Chellali, Di Wang, Leonardo Velasco, Ruby Singh, Thomas Reisinger, Robert Kruk,* and Horst Hahn*

Nanocomposite materials, consisting of two or more phases, at least one of which has a nanoscale dimension, play a distinctive role in materials science because of the multiple possibilities for tailoring their structural properties and, consequently, their functionalities. In addition to the challenges of controlling the size, size distribution, and volume fraction of nanometer phases, thermodynamic stability conditions limit the choice of constituent materials. This study goes beyond this limitation by showing the possibility of achieving nanocomposites from a bimetallic system, which exhibits complete miscibility under equilibrium conditions. A series of nanocomposite samples with different compositions are synthesized by the co-deposition of 2000-atom Ni-clusters and a flux of Cu-atoms using a novel cluster ion beam deposition system. The retention of the metastable nanostructure is ascertained from atom probe tomography (APT), magnetometry, and magnetotransport studies. APT confirms the presence of nanoscale regions with ≈100 at% Ni. Magnetometry and magnetotransport studies reveal superparamagnetic behavior and magnetoresistance stemming from the single-domain ferromagnetic Ni-clusters embedded in the Cu-matrix. Essentially, the magnetic properties of the nanocomposites can be tailored by the precise control of the Ni concentration. The initial results offer a promising direction for future research on nanocomposites consisting of fully miscible elements.

1. Introduction

Tailoring functional properties of materials often requires control over their complex microstructure containing several phases. Alloys containing metallic precipitates or non-metallic dispersions embedded in metallic matrices are highly sought-after microstructures in structural applications. For example superalloys and dispersion-strengthened alloys, retain their high strength and low creep rates even when exposed to high temperatures due to their engineered microstructure.[1–4] In addition, a combination of high mechanical strength and low electrical resistivity, critical for advanced electrical conductors, can be obtained in a two-phase structure consisting of nanometer-sized precipitates in a matrix.[5,6] Similarly, high-performance magnetic materials and superconducting materials can benefit from two-phase structures with one phase being finely dispersed nanometer-sized particles.[7–10] However, thermodynamic and processing

G. Iankevich, T. Reisinger, H. Hahn
Institute for Quantum Materials and Technologies
Karlsruhe Institute of Technology
Hermann-von-Helmholtz-Platz 1
76344 Eggenstein-Leopoldshafen, Germany
E-mail: gleb.andreevich@kit.edu

G. Iankevich, A. Sarkar, S. Katnagallu, M. R. Chellali, D. Wang, L. Velasco, R. Singh, T. Reisinger, R. Kruk, H. Hahn
Institute of Nanotechnology
Karlsruhe Institute of Technology
Hermann-von-Helmholtz-Platz 1
76344 Eggenstein-Leopoldshafen, Germany
E-mail: robert.kruk@kit.edu

The ORCID identification number(s) for the author(s) of this article can be found under https://doi.org/10.1002/adma.202208774.

DOI: 10.1002/adma.202208774

A. Sarkar, H. Hahn
KIT-TUD Joint Laboratory Nanomaterials
Technical University Darmstadt
64287 Darmstadt, Germany

S. Katnagallu
Department of Computational Materials Design
Max Planck Institut für Eisenforschung GmbH
Max-Planck- Str. 1, 40237 Düsseldorf, Germany

M. R. Chellali, D. Wang
Karlsruhe Nano Micro Facility
Karlsruhe Institute of Technology
Hermann-von-Helmholtz-Platz 1
76344 Eggenstein-Leopoldshafen, Germany

L. Velasco
Direccion Academica
Universidad Nacional de Colombia Sede de La Paz
Km 9 via Valledupar-La Paz, Cesar 202017, Colombia

constraints typically limit the range of size and distribution of precipitates/dispersions and their volume fraction.

In order to achieve metal–metal multiphase nanoparticle-dispersed structures (nanocomposites) in thin films, advanced physical vapor deposition (PVD) methods such as magnetron sputtering, pulsed laser deposition, thermal or e-beam evaporation etc., sometimes in combination with each other and other materials post-processing techniques have been used.[11] Usually, in these PVD techniques two or more elements with no or limited miscibility, according to the equilibrium phase diagram, are co-deposited. This limited miscibility leads to the formation of precipitates (clusters) of one element in the matrix of the other in the growing film and depending on the specific processing parameters during the deposition.[12–15] Nevertheless, controlling the structure of the material, precipitate's size, their distribution, and materials relative composition, still remains a difficult task due to the nature of the material system and limitations of synthesis techniques.

A way to overcome these limitations is the simultaneous deposition of well-defined nanoparticles/clusters together with an atomic flow of another material as a matrix in a controlled environment. Commonly, pre-formed clusters in a form of an ion beam can be guided from their source toward the deposition surface. Several different methods such as gas aggregation, laser evaporation, and pulsed arc sources are established and can act as a source of clusters.[16–19] Then by controlling the deposition energy of the clusters and the flow of the co-deposited materials, it is possible to control the structure of the resulting material, that is, tune the resulting material properties.[20] Previously, such systems already demonstrated the ability to synthesize a wide variety of materials suitable for scientific studies but the industrial application is limited by the ion beam intensity that has to be increased, or alternative methods need to be developed.[21]

An in-house ultrahigh vacuum (UHV) cluster ion beam deposition (CIBD) system was purposely designed and built at the Institute of Nanotechnology.[22] The CIBD system overcomes the limitations of other synthesis techniques, especially in the ability to control the size and size distribution of the clusters, choose the materials combinations, and deposit size-selected clusters containing tens to a few thousand atoms per cluster. The clusters can be either embedded at any targeted volume fraction in a matrix of another element, or solely be synthesized as cluster-based thin films. The material combinations that have so far been prepared, using the CIBD deposition system, typically consist of elements with a rather low solubility, such as Fe-clusters in Ag-, Ge-, or Cr-matrix.[23–25] The structure and the physical properties of these clusters–matrix combinations have been characterized using advanced techniques such as transmission electron microscopy (TEM), atom probe tomography (APT), superconducting quantum interference device (SQUID) measurement, and physical property measurement system (PPMS) measurement. The flexibility and ability of the CIBD system to synthesize complex cluster-assembled materials with high precision allows their integration into more sophisticated magnetic Fe–Ge–Nb-based Josephson junctions. Such junctions have been studied in an advanced application in neuromorphic computing.[26]

The preparation of the metal–metal multiphase nanocomposites made of a fully miscible material system is less straightforward. So, in order to expand the materials combinations to include fully miscible elements and to establish the potential of such systems for functional properties, the Ni–Cu system was chosen for the present study. Ni–Cu system is one of the most intensively studied binary metallic systems demonstrating a complete miscibility. Consequently, Ni–Cu alloys find applications in various fields of science and technology, for example in magnetic devices, as catalysts, corrosion resistant structural materials, etc.[27,28] Here, the choice of Ni as a ferromagnetic metal for the clusters facilitates additional magnetic measurements allowing to obtain valuable information on the cluster state and their distribution within the matrix.[29,30] Here, Ni-clusters were embedded in a Cu-matrix, which is simultaneously co-deposited from a separate thermal evaporation source. Full control of the size and volume fraction of the Ni-clusters in the Cu-matrix is possible by adjusting the respective cluster size and the ratio of the flux of the cluster beam (Ni) and/or of the atomic flux (Cu). In thermodynamic equilibrium, any combination of Ni-clusters in a Cu-matrix is not stable, thus, the clusters are deposited on a liquid N_2 cooled substrate to reduce interdiffusion during the preparation. In order to evaluate the evolution of the structural and physical properties, a stepwise annealing procedure at elevated temperatures was performed.

2. Results and Discussion

The CIBD system, shown schematically in **Figure 1**, is a state-of-the-art in-house designed and built UHV system for the deposition of clusters onto a substrate simultaneously with a matrix material. Thy system allows for precise control of cluster size, size distribution, and their impact energy. Detailed information on the CIBD system and the possible morphologies of deposited cluster-based thin films has been previously reported.[22,24] For cluster-based nanocomposite systems, such as the Ni-clusters embedded in a Cu-matrix presented in this work, the

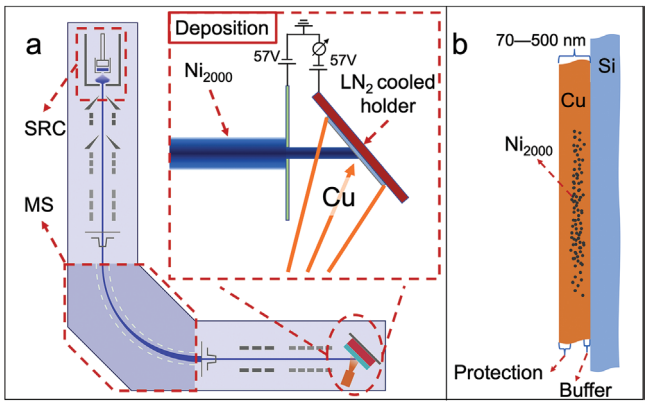

Figure 1. a) Schematic drawing of the CIBD system and the deposition stage, consisting of the cluster source (SRC), and the mass separation unit (MS). The deposition stage used in this work is enlarged in the inset to show the incoming Ni-cluster beam and the Cu-atom flux from a separate effusion cell evaporation source. The deposition stage allows the deposition of a wide concentration range of Ni-clusters within the Cu-matrix, by correspondingly adjusting the cluster and the atom fluxes. b) The sequence of layers with the Ni_{2000} clusters embedded in the Cu-matrix grown on an Si-substrate is shown schematically.

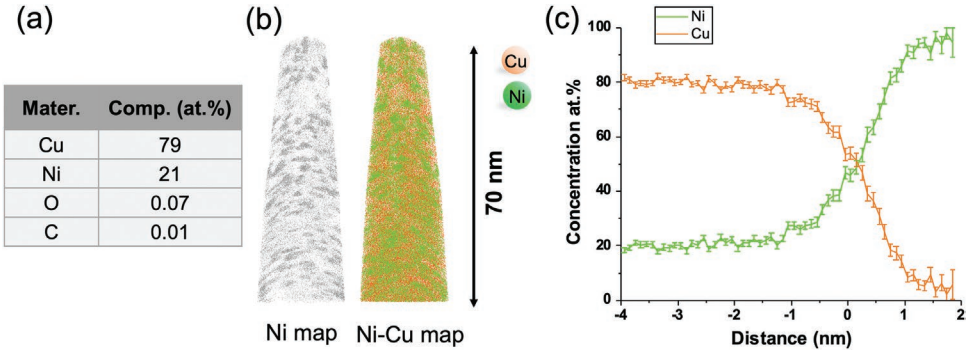

Figure 2. APT data for the cluster nanocomposite containing 21 at% Ni. a) Sample composition data, b) 3D reconstructions of APT volumes, left: representation of Ni atoms only, right: representation with colored Ni and Cu atoms, c) proximity histogram averaged over several clusters in the analyzed volume.

nanocomposite composition, that is, Ni atomic concentration (at%), within the matrix can be varied over a wide composition range, irrespective of the corresponding equilibrium Ni–Cu phase diagram.[31] Of course, the thermal stability of the resulting metastable structure, especially at elevated temperatures, is an important feature that needs to be studied by simulation and/or experiment for each selected nanocomposite system.

The clusters exit the source with a single negative charge (Figure 1a, SRC), and have a lognormal size distribution and an energy distribution of a few eV. Therefore, prior to the deposition onto the substrate, the clusters are mass-separated (with a final mass distribution ±10%) by means of a 90° sector magnet (Figure 1a, MS (Danfysik, Denmark, custom design, nominal radius 500 mm, maximum magnetic flux density 1.4 T)).

The deposition stage (Figure 1a, inset deposition) allows for the precise control of the impact energy of the charged cluster ions onto the substrate. In the present study, the clusters were deposited in the soft-landing mode (with an energy of 57 eV per cluster) in order to reduce or prevent their deformation or even destruction. For the co-deposition of the Cu-matrix, a high-temperature effusion cell (CreaTec Fischer & Co., HTC) is used. In order to reduce the cluster mobility on the surface and to prevent or minimize the formation of cluster aggregates, as well as reduce the atomic diffusion during the formation of the nanocomposite, the substrate is cooled to ≈140 K by using a liquid-nitrogen-cooled substrate holder. For the present study, an initial series of experiments was performed in order to calibrate the CIBD system and determine the specific deposition parameters. The parameters of the clusters source were calibrated in order to achieve the maximum flux of the ion beam for the selected cluster size. The cluster size was selected based on considerations of detectability of the clusters using APT and magnetometry. Additionally, the deposition parameters were optimized to reduce the intermixing of the clusters with the matrix during the deposition process and to avoid the deformation of the clusters during the landing on the sample surface.

Here, the CIBD system was adjusted to prepare Ni-clusters consisting of 2000 atoms (±10%, Ni_{2000}). A schematic drawing of the cross-section of the sample prepared by CIBD is shown in Figure 1b. The active nanocomposite layer, containing the Ni-clusters, was protected from coming in contact with the Si-substrate (buffer) and from being exposed to the environment (protection) by Cu-layers on both sides. The protection and the buffer layers had thicknesses of 50 and 20 nm, respectively. Assuming the bulk density the size of a single Ni_{2000} cluster is calculated to be ≈3.5 nm in diameter with approximately 38% of Ni atoms residing on the cluster surface. A series of cluster-assembled nanocomposite samples with different concentrations of Ni within the Cu-matrix (between ≈2 and ≈22 at%) were prepared.

Two representative samples were analyzed using APT. The distribution of Ni and Cu atoms for both samples is shown in **Figures 2** and **3** for 21 at% and 2.6 at% Ni in Cu, respectively. For both samples, a granular-like morphology is observed in the as-prepared condition with well-defined regions of high Ni and/or Cu concentration. In certain regions, the Ni-concentration reaches up to ≈100 at%. For the 21 at% sample, a composition profile is presented in Figure 2c as a proximity histogram. The analysis was performed for several clusters within the analyzed region and subsequently averaged. From this analysis, it is concluded that the analyzed clusters reach ≈100 at% concentration of Ni, clearly confirming the presence of clusters with high Ni-concentration. Clearly, the Ni-clusters remain intact during the preparation at low temperature and the subsequent treatment, that is, storage and preparation of the APT-tip, performed at room temperature. Also, APT reveals that the average concentration of Ni remains at ≈20 at% within several nm around the clusters, that is, indicative of the formation of an NiCu solid solution at the cluster–matrix interfaces. Regions reaching ≈100 at% of Cu content within the analyzed volume as well as clusters formed a solid solution of various compositions also were observed and more information can be found in the Supporting Information (Figure S2, Supporting Information).

Furthermore, the APT data demonstrated that the oxygen and carbon content in the as-prepared samples was low (<0.1 at% for O and C for both samples, Figures 2a and 3a) despite the relatively large distance of ≈4 m traveled by the individual cluster ions in the beamline. After preparation, the samples were removed from the CIBD system and transported under normal atmospheric conditions for further processing. During transport, the samples were exposed to a maximum temperature of 25 °C. The purity of the samples shows the cleanliness of the CIBD system and the effectiveness of the capping Cu layer in protecting the Ni-clusters against oxidation.

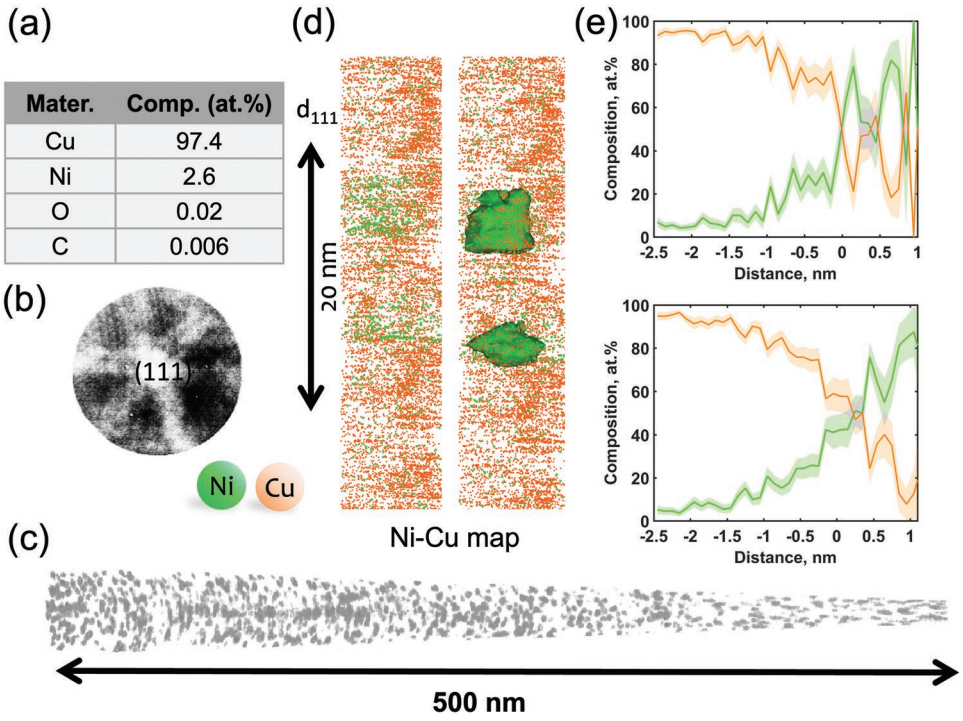

Figure 3. APT results for a 2.6 at% sample. a) Sample composition data, b) detector event histogram allowing the precise scale calibration, c) Ni map d) reconstruction of a local Cu phase with embedded Ni_{2000} clusters. e) Proximity histograms on the right demonstrate the composition of the located Ni-clusters.

Figure 3 presents the APT analysis of the sample with 2.6 at% Ni concentration. As shown in Figure 3a the composition of Ni and Cu match well with the aimed cluster compositions during synthesis. The detector event histogram as shown in Figure 3b presents a threefold symmetry consistent with the (111) crystallographic direction of an fcc material, indicating that the analyzed volume in APT had only one Cu grain. Using the crystallographic information from the detector event histogram we were able to reconstruct sub-volumes of the APT data with resolved (111) lattice planes. Along with the Cu lattice planes, two Ni-clusters can be seen coherently embedded in the Cu-matrix, in Figure 3d. The 1D composition profiles, plotted in Figure 3e, for these two clusters demonstrate the partial dissolution of Ni-clusters. The Cu content between the clusters reaches ≈100 at%, demonstrating that the clusters are indeed well separated by the matrix. Figure 3c shows a reconstructed Ni map of the sample, where Ni-clusters are observed within the entire thickness (≈500 nm) of the nanocomposite.

The APT analysis (Figures 2 and 3) and the derived overall elemental composition illustrates the precision and reproducibility of the CIBD system for attaining the desired Ni composition in the nanocomposite. The composition is controlled by the flux of the single-charged clusters, that is, the ion current, and the deposition rate of the Cu-matrix from the effusion cell. For example, the deposition parameters for the samples shown in Figures 2 and 3 were respectively set to yield 20 at% and 2.5 at% of Ni-clusters, respectively, well confirmed by APT.

Besides determining the overall composition of the nanocomposite, APT was crucial to yield information regarding the metastability of the obtained structures and the presence of regions with ≈100 at% Ni within the Cu-matrix in both samples.

Magnetic property measurements of the Ni/Cu nanocomposites show their magnetic behavior and provide further evidence for the presence of the Ni-clusters at different concentrations. Like for other ferromagnetic materials, Ni-clusters are single-domain magnets below a critical cluster (nanoparticle) size. For pure Ni, the critical size has been reported to be 21.2 nm.[32] Below the ferromagnetic transition temperature (Curie temperature, T_C) down to the blocking temperature (T_B), a single-domain cluster can be considered as a superparamagnet with all its magnetic moments collectively fluctuating under thermal excitations. Further cooling below T_B results in slowing down the fluctuations of the magnetization. In this temperature range, during the measurement time, the magnetic moment appears to be frozen in one direction and the cluster ensemble behaves again as a ferromagnet. It is known that the blocking temperature of cluster assemblies is influenced by many factors such as magnetic anisotropy of the clusters, their size, or intracluster dipole–dipole interactions (distance dependent). Thus, the variation of the cluster size and/or concentration is expected to be associated with a respective change of T_B. Consequently, using VSM-SQUID magnetometry, the blocking temperatures T_B were determined by applying the field-cooled (FC) and the zero-field-cooled (ZFC) protocols to the nanocomposite samples. The blocking temperature T_B is defined as a peak of the ZFC curve, that is, where the system undergoes the superparamagnetic-ferromagnetic transition. Generally, not only the value of T_B but also the shape of the FC/ZFC curves depends on several factors such as particle size, size distribution, interparticle distances, interaction with the matrix material, etc.

To find a relationship between the different concentrations of Ni-clusters and the magnetic characteristics of the Ni/Cu

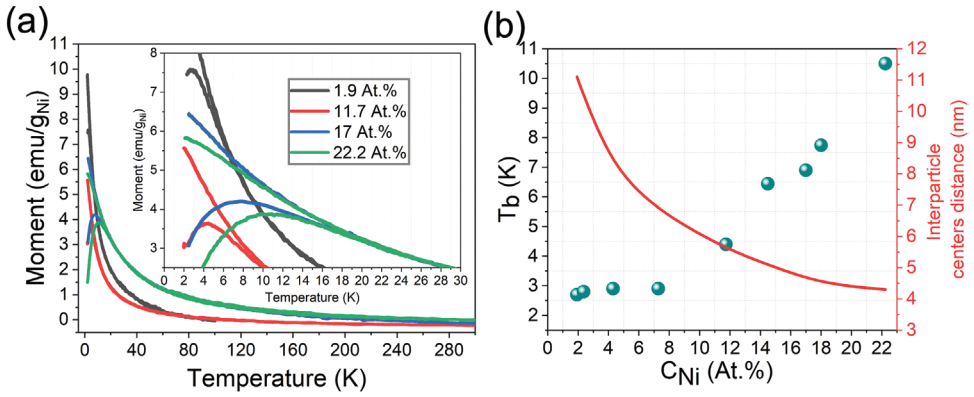

Figure 4. Results of the VSM SQUID magnetometry: a) ZFC/FC measurements for Ni/Cu cluster/matrix nanocomposites for different compositions of 1.9, 11.7, 17.0, and 22.2 at% Ni. b) Dependence of the blocking temperature T_B for all Ni-concentrations (see Figure S1, Supporting Information), as determined from ZFC/FC magnetic measurements in (a), as a function of the Ni-concentration C_{Ni}. In addition, the calculated average interparticle distance is plotted as a function of C_{Ni}, with values ranging from ≈4 nm to 11.5 nm.

cluster/matrix nanocomposites, a series of SQUID magnetometry measurements were carried out. Some representative ZFC/FC curves are shown in **Figure 4**a, for samples with Ni concentrations of 1.9, 11.7, 17, and 22.2 at%, respectively. The ZFC/FC curves of all samples are presented in the Supporting Information (Figure S1, Supporting Information). All measurements were performed with an applied external field (H) of 100 Oe. As mentioned previously, the shape of the ZFC/FC curves as well as their divergence is a clear indication of the presence of single-domain magnetic clusters in the as-prepared samples, providing independent evidence for the presence of Ni-clusters in the fully miscible Ni-Cu nanocomposite system. As seen in Figure 4a, the blocking temperatures T_B for the samples with compositions from 1.9 to 22.2 at% range from 2.7 K to nearly 11 K.

In Figure 4b (solid dots) the dependence of T_B on the concentration of Ni-clusters in the Cu-matrix is shown together with the average distances between cluster centers, which were calculated by assuming a cubic cluster arrangement. This way, as a first approximation, one introduces a cluster–cluster distance as a parameter for the characterization of the nanocomposites. It should be pointed out here that in reality, the Ni-clusters land randomly onto the substrate and then they become embedded within the Cu-matrix. Consequently, the probability of the clusters forming agglomerates, increases with increasing Ni-clusters concentration. Moreover, from the APT data, it was evident that some clusters in the as-prepared state start to form a local NiCu solid solution of various concentrations.

For the dilute samples, that is from ≈2 up to ≈7 at% Ni concentration, a plateau in the T_B dependence versus Ni-concentration is observed (Figure 4b). In this compositional range, the clusters are sufficiently far apart (i.e., ≈11–6.5 nm average distance between the centers of the particles) and, thus, the effect of magnetic dipole–dipole interactions between the clusters can be neglected. In the region between ≈12 and ≈18 at% (i.e., ≈6.5–5.5 nm average distance between the centers of the particles), T_B rises steeply with decreasing intercluster distances. The steep increase of T_B is most likely due to the significant contribution by the dipole–dipole interactions, which are strongly distance-dependent. The trend of increasing T_B continues even at the highest concentration (up to 22 at%) of Ni-clusters, with an average cluster–cluster distance of 4.2 nm for an average cluster size of 3.5 nm, that is, when the clusters almost touch each other. In addition, the shapes of the ZFC curves also provide some indication of the cluster arrangement in the matrix. The relatively narrow cusps in the ZFC curves of the low concentration samples indicate well-spaced clusters with a narrow size distribution. On the other hand, the broadening of the ZFC cusps, observed with increasing Ni-clusters concentration, suggests the presence of strong dipole–dipole interactions and/or formation of cluster agglomerates during the cluster deposition process.

In conclusion, the results of the elemental mapping using APT and of the magnetic studies of the as-prepared nanocomposite samples provide convincing evidence for the presence of Ni-clusters distributed within the Cu-matrix. The Ni-clusters are well-preserved, with some dissolution of Ni into the Cu-matrix, as observed in the proximity histograms (Figures 2c and 3e). Considering the complete miscibility of the constituents, the nanocomposites are in a highly metastable state. However, at room temperature, the metastable state is preserved due to the limited diffusion between the constituents. The remaining important question of the temperature/time range over which the metastable state can be stabilized is addressed in the following section.

The stability range of Ni-clusters in a Cu-matrix at elevated temperatures was studied in gradual annealing experiments. The resulting structural changes of the clusters were examined using complementary techniques: in addition to the APT analysis and the characterization of the magnetic properties (saturation magnetization, and superparamagnetic blocking temperature, T_B), the magnetoresistivity of the samples was measured to obtain additional insight regarding the structural changes occurring during the temperature treatment. Based on the evidence of separated single-domain superparamagnetic Ni-clusters within the conducting Cu-matrix, it is anticipated that magnetoresistance (MR) should be observed,[33] due to the spin-dependent scattering of the electrons at the superparamagnetic clusters. For such cluster-based Ni–Cu nanocomposites, no MR response has been previously reported due to the complexity of the synthesis of such systems. However, MR effects in Ni–Cu

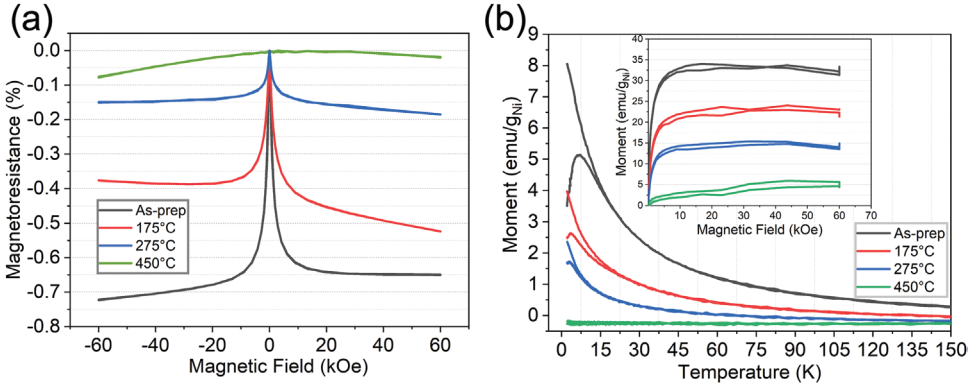

Figure 5. Magnetoresistance and magnetic properties of the samples with Ni-concentration of 17 at% in the as-prepared and the annealed state. a) MR (H_{app}) measured at 10 K; b) $M(T)$ and $M_s(H_{app})$ measured at 10 K.

multilayers have been already been studied by Bird et al.[34] and by Vikram et al.[35]

Here, it is worth noting that the samples for the MR studies required a different design than those used for both the APT and magnetic measurements. The modification was needed to ensure that the applied current only flows across the nanocomposite in the MR measurement, making sure that only negligible amounts of shunt current flow through the protective and buffer layers (composed of pure Cu). For this reason, these two Cu-layers were significantly reduced in thickness. Consequently, the thickness of the buffer layer was chosen to be only 2.5 nm and that of the protective layer to be 4 nm. The total thickness of the nanocomposite layer was about 80 nm, that is, 90% of the total thickness, with the Ni-concentration in this region being ≈17 at%. All samples were annealed in a vacuum furnace (base vacuum < 8×10^{-8} mbar) first at 175 °C (448 K), then at 275 °C (548 K), and finally at 450 °C (723 K) for 2 h each sequentially.

The results of the MR measurements carried out at 10 K with an applied magnetic field, H_{app}, up to 6 T, are shown in **Figure 5**. The as-prepared sample exhibits a negative magnetoresistance at low temperatures (Figure 5a). The magnitude of the MR effect decreases significantly upon successive annealing steps at elevated temperatures and vanishes completely after annealing at 450 °C for 2 h. These results confirm the expected disappearance of the magnetic Ni-clusters by interdiffusion of Ni and Cu. At the highest annealing temperature, spin-dependent electron-scattering entities are absent and, consequently, no MR effect is observed.

Additionally, the annealing effects on the saturation magnetization and blocking temperature (Figure 5b) were measured using a sample with a Ni-concentration of 17 at%. The $M(H)$ curves, shown in the inset of Figure 5b, were also measured at 10 K. At this temperature, no coercivity was observed, even on the as-prepared sample, because the Ni-clusters remain in the superparamagnetic state (T_B is lower than 10 K). As can be seen from Figure 5b, the magnetization and blocking temperature decrease with increasing annealing temperatures. This trend is the result of the decreasing magnetization caused by the gradual dissolution of the Ni-clusters by the intermixing of Ni and Cu. At the intermediate annealing temperatures of 175 and 275 °C, the Ni and Cu interdiffusion results in the partial dissolution of the Ni-clusters and thus in a decrease of the magnetic moments of the clusters. The continued interdiffusion results in a weakening of the ferromagnetic order, eventually leading to a paramagnetic state. Ultimately, after annealing at 450 °C the ZFC/FC curves the $M(H)$ loops show the distinctive characteristics of a material in a paramagnetic state.

Direct evidence for the dissolution of the Ni-clusters and for the formation of an NiCu solid solution during annealing is also obtained from the APT characterization on a sample with 21 at% Ni-concentration. The changes of the Ni- and Cu-distribution in the as-prepared sample in comparison with those after annealing at 275 and 450 °C for 2 h are shown in **Figure 6**. From the data presented in Figure 2b for the as-prepared sample with 21 at% Ni, the distribution of the Ni–Ni pair distances was calculated as shown in Figure 6a. The Ni–Ni pair distribution is distinctly different from that obtained assuming a randomized distribution of the Ni-atoms in the Cu-matrix as theoretically calculated. It is evident that the Ni–Ni pair distribution is significantly narrower than the random distribution. Furthermore, the Ni–Ni pair distances are shifted to lower values (compared to the randomized counts). These observations are in agreement with the presence of pristine Ni-clusters and regions of substantial Ni-enrichment as expected for distinct clusters. Figure 6a represents the data obtained from the sample annealed at 275 °C for 2 h. The peak of the experimental Ni–Ni-pair distribution shifts toward the randomized distribution as a result of the beginning mixing of the Ni- and Cu-atoms by interdiffusion, yet still not fully overlapping with the randomized counts. It can be concluded from this analysis that even after annealing at 275 °C, regions with relatively high Ni-concentrations and correspondingly closer Ni–Ni-distances do persist. This observation is corroborated by the magnetic properties for the sample with the same Ni-concentration, namely a relatively low T_B around 3.1 K (Figure 5b). The APT elemental maps for the samples annealed at 275 °C is presented in the Supporting Information (Figure S3, Supporting Information).

As seen in the elemental distribution map shown in Figure 6b and from the complete overlap of the Ni–Ni pair distances (Figure 6a) with the distribution for a randomized sample, Ni is evenly distributed over the entire analyzed volume after annealing at 450 °C for 2 h. Small fluctuations of the composition with lower Ni content are observed at both ends of the ana-

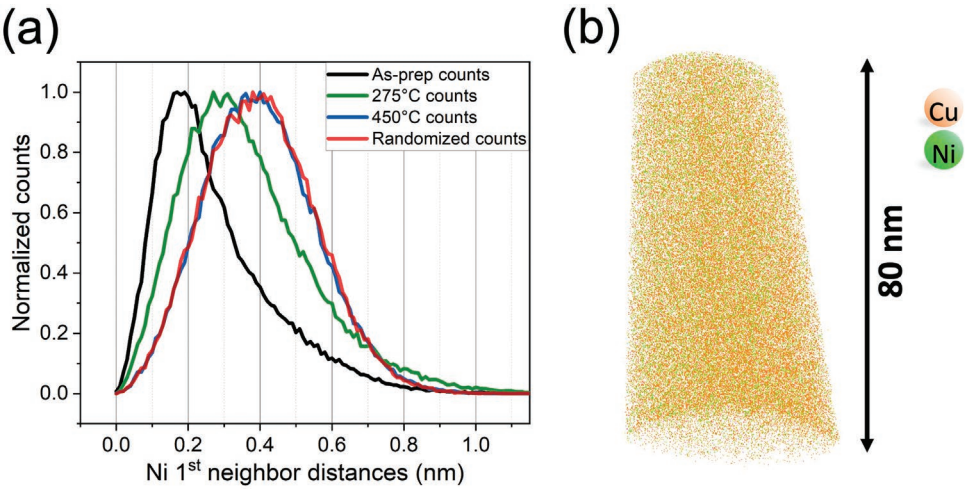

Figure 6. Results of APT measurements. a) The evolution of the Ni–Ni-pair distances calculated for an as-prepared sample and for the sample after annealing at 275 and 450 °C for 2 h with an Ni-concentration of 21 at%. b) Elemental distribution reconstruction of Ni and Cu after annealing at 450 °C for 2 h from APT.

lyzed region, most likely caused by the buffer and capping layers of the sample (Figure S4, Supporting Information). The oxygen level in the entire sample remains negligible (less than 0.1 at%), even after the high-temperature annealing, demonstrating the overall cleanliness of all the steps including the sample preparation, its subsequent annealing, and APT measurements.

The annealing at 450 °C results in the complete dissolution of the Ni-clusters, as expected from the fully miscible phase diagram. A homogeneous NiCu solid solution with ≈20–21 at% Ni composition is obtained. The complete disappearance of the ferromagnetic order and the transition to a paramagnetic state as expected for an $Ni_{20}Cu_{80}$ alloy further confirms the APT results.[36]

The observation of the partial and then complete dissolution of Ni-clusters in the Cu-matrix after annealing at 275 and at 450 °C, respectively, is consistent with the temperature range estimated from the interdiffusion coefficients for the Ni–Cu system.[37] The values of diffusional length $(D_t)^{1/2}$ for $t = 7200$ s at 275 °C (548 K) and 450 °C (723 K) are 60 nm and 380 nm, respectively. In particular, the value at 450 °C is large enough to allow complete homogenization of the sample, as experimentally observed in this study.

3. Conclusions

The present work demonstrates the possibility of preparing a metastable nanocomposite material consisting of size-selected Ni-clusters embedded in a Cu-matrix, which under equilibrium conditions is a fully miscible system , using an in-house designed state-of-the-art CIBD system.

The versatility and adaptability of the CIBD system opens the possibility to prepare nanocomposites composed of clusters made of ≈2000 Ni atoms (with a diameter of ≈3.5 nm) with overall Ni concentrations ranging from ≈2 to ≈22 at%. The presence of the Ni-clusters and their stability in the as-prepared state and under moderate annealing conditions are demonstrated by mapping the elemental distribution using the APT and measuring magnetic and magnetoresistive properties. In particular, APT shows the presence of well-defined local zones with Ni concentrations reaching ≈100% for both low (2.6 at%) and high (21 at%) Ni concentrations.

The magnetic properties of the as-deposited samples are found to be related to the concentration of Ni-clusters. For relatively small concentrations up to ≈8 at% the Ni-clusters behave as well-separated single-domain ferromagnetic/superparamagnetic entities. At higher concentrations, that is, as the distance between clusters decreases, there is evidence of strong magnetic dipole–dipole interactions that strongly influence the superparamagnetic properties.

Furthermore, the gradual Ni–Cu intermixing and the stability limits of Ni-clusters are probed using APT, as well as magnetic and magnetotransport measurements in samples annealed under UHV conditions. It is found that stepwise annealing of the 21 at% nanocomposite at 175 °C, 275 °C for 2 h successively leads to gradual dissolution of Ni-clusters in the Cu-matrix. Even after annealing at 275 °C regions of high Ni concentration remain, as confirmed by magnetic and APT measurements. Finally, after subsequent annealing at 450 °C for 2 h, the formation of a homogeneous NiCu solid solution of 20–21 at% composition is observed.

In the present study, using the advantages of the CIBD technique, the potential combinations of materials in nanocomposites have been greatly expanded to include fully miscible systems such as Ni–Cu. Such systems based on metastable nanocomposites can find applications, especially at low temperatures, in magnetic, sensing, and quantum devices. It is envisioned that the CIBD technique can be integrated into more complex fabrication processes requiring a precise control over the synthesis parameters.

4. Experimental Section

In the CIBD system, a Haberland type[21,38,39] cluster source, based on the combination of the magnetron sputtering and inert gas aggregation (Figure 1a, SRC), was employed for the synthesis of pure

Ni-clusters under a controlled atmosphere in the source section and ultrahigh vacuum (UHV) conditions in the remaining part of the system. As a sputtering target, a 99.99% pure Ni target was used (Kurt J. Lesker Company Ltd.) and sputtering power was fixed to 70 W. The base pressure in the aggregation chamber (Figure 1a, SRC) was $\approx 2 \times 10^{-8}$ mbar, and backfilled during cluster synthesis with a mixture of Ar and He gas to ≈2 mbar (Ar gas flow of 110 sccm, He gas flow of 110 sccm). In the deposition chamber the base pressure was 2×10^{-10} mbar range and remained in 5×10^{-9} mbar range during the entire deposition process. Most importantly, the present research clearly showed that the UHV-conditions prevented the oxidation of the clusters and protected them effectively against other types of contamination.

The advanced deposition stage (Figure 1a, Deposition) was designed in such a way that the area for the deposition of the clusters is smaller than the area for the deposition of the matrix material. The angle between the cluster ion beam and the atomic flow originating from the effusion cell was 70° (Figure 1a, Deposition), so the deposition of clusters and matrix material occurred at equal angles of 35° each.

The cluster ion current was measured with a help of a pico-amperemeter (Keithley, 6400 series). Based on the desired cluster concentration (at% of Ni in Cu), the temperature of the effusion cell was adjusted to obtain the necessary Cu-flux. Cu pellets (99.99% pure Kurt J. Lesker Company Ltd.) were used as a source of the matrix material. The Cu-flux was continuously measured using a calibrated quartz crystal monitor.

The nanocomposite films were deposited on silicon substrates (Figure 1b, (100, p-type)), with a size by 5 × 5 mm and a thickness of 0.3 mm with a native oxide layer. Prior to the sample deposition, each silicon substrate was subjected to a two-step cleaning process, first with snow-jet cleaning (Tectra GmbH) and then in oxygen plasma (Oxford Plasma 80 RIE system) processed for 2 min at 30 W and 15 sccm of O_2 at a pressure of 0.1 mbar. The samples were mounted on Omicron-type sample holders together with a custom-designed mask and loaded through a sample loading chamber (base pressure $<5 \times 10^{-8}$ mbar), from where they were transferred in situ to the deposition chamber using an UHV manipulator.

The samples for the APT were prepared in the form of sharp needles, using Focused Ion Beam (FIB) Strata 400 instrument (FEI).[40] The radius for all APT tips was less than 50 nm. APT was performed on a Local Electrode Atom Probe (LEAP) 4000 HR instrument (Cameca). The measurements were carried out using a pulsed laser of energy 50 pJ, repeated at 120 kHz. The base temperature of the tips during the APT measurements was kept at 50 K. A virtual 3D reconstruction and further compositional analysis were made using the IVAS 3.8.2 software package and graphs were plotted using MATLAB 2019b.

The study of the magnetic properties for the determination of the superparamagnetic blocking temperature (T_B) and saturation magnetization (M_S) of the nanocomposite films was performed using a vibrating sample magnetometer superconducting quantum interference device (VSM-SQUID, MPMS3, Quantum Design). T_B was measured using zero-field-cooled/field-cooled (ZFC/FC) curves as a function of temperature with an applied magnetic field of H = 100 Oe. The measurements of M_S were carried out at different temperatures (300 K, 100 K, 10 K, 5 K, 2.5 K, and 2 K) with an applied magnetic field up to 6 T.

The magnetotransport properties were studied using a Physical Properties Measurement System (PPMS, Quantum Design) using the 4-points measurement technique at 10 K and maximum applied magnetic field of 6 T. Measured samples were post-processed using the Nd–YAG laser with a laser beam diameter of 20 µm and frequency of 800 kHz (TRUMPF Gmbh. TruMicro 5000) in order to cut out the specific region of the deposited nanocomposite film to which the conduction wires were bonded to.

Supporting Information

Supporting Information is available from the Wiley Online Library or from the author.

Acknowledgements

The authors acknowledge Dr. Virgil Provenzano for his support and help during this manuscript preparation. G.I. acknowledges Dr. Evgeniy Boltynjuk and Ramin Shadkam for their assistance during the work. H.H. is grateful to the State of Hesse for an equipment grant to build the CIBD system.

Open access funding enabled and organized by Projekt DEAL.

Conflict of Interest

The authors declare no conflict of interest.

Data Availability Statement

The data that support the findings of this study are available from the corresponding author upon reasonable request.

Keywords

bimetallic systems, cluster science, nanocomposites, nickel–copper systems, superparamagnetism

Received: September 23, 2022
Revised: November 9, 2022
Published online:

[1] J. H. Weber, M. K. Banerjee, in *Reference Module in Materials Science and Materials Engineering*, Elsevier, Amsterdam, The Netherlands **2016**.
[2] H. Clemens, S. Mayer, C. Scheu, in *Neutrons and Synchrotron Radiation in Engineering Materials Science*, John Wiley & Sons, Ltd., Hoboken, NJ, USA **2017**, pp. 1–20.
[3] J. S. Benjamin, *Metall. Mater. Trans. B* **1970**, *1*, 2943.
[4] R. Casati, M. Vedani, *Metals* **2014**, *4*, 65.
[5] L. Ye, Z. Lai, J. Liu, A. Tholen, *IEEE Trans. Electron. Packag. Manuf.* **1999**, *22*, 299.
[6] G. R. Ruschau, S. Yoshikawa, R. E. Newnham, *J. Appl. Phys.* **1992**, *72*, 953.
[7] A. Gerber, A. Milner, B. Groisman, M. Karpovsky, A. Gladkikh, A. Sulpice, *Phys. Rev. B* **1997**, *55*, 6446.
[8] N. Moutalibi, A. M'chirgui, J. Noudem, *Phys. C Supercond.* **2010**, *470*, 568.
[9] M. L. Schneider, C. A. Donnelly, S. E. Russek, B. Baek, M. R. Pufall, P. F. Hopkins, P. D. Dresselhaus, S. P. Benz, W. H. Rippard, *Sci. Adv.* **2018**, *4*, e1701329.
[10] L. Grünhaupt, M. Spiecker, D. Gusenkova, N. Maleeva, S. T. Skacel, I. Takmakov, F. Valenti, P. Winkel, H. Rotzinger, W. Wernsdorfer, A. V. Ustinov, I. M. Pop, *Nat. Mater.* **2019**, *18*, 816.
[11] P. H. C. Camargo, K. G. Satyanarayana, F. Wypych, *Mater. Rep.* **2009**, *12*, https://doi.org/10.1590/S1516-14392009000100002.
[12] S. Zhang, N. Ali, *Nanocomposite Thin Films and Coatings: Processing, Properties and Performance*, Imperial College Press, London, UK **2007**.
[13] S. C. Velasco, A. Cavaleiro, S. Carvalho, *Prog. Mater. Sci.* **2016**, *84*, 158.
[14] S. Zhang, D. Sun, Y. Fu, H. Du, *Surf. Coat. Technol.* **2003**, *167*, 113.
[15] K. Lukaszkowicz, *Review of Nanocomposite Thin Films and Coatings Deposited by PVD and CVD Technology*, IntechOpen, London, UK **2011**.

[16] C. Binns, *Surf. Sci. Rep.* **2001**, *44*, 1.
[17] Y. Xu, Z. G. Sun, Y. Qiang, D. J. Sellmyer, *J. Appl. Phys.* **2003**, *93*, 8289.
[18] Y. Xu, Z. G. Sun, Y. Qiang, D. J. Sellmyer, *J. Magn. Magn. Mater.* **2003**, *266*, 164.
[19] J. M. Meldrim, Y. Qiang, Y. Liu, H. Haberland, D. J. Sellmyer, *J. Appl. Phys.* **2000**, *87*, 7013.
[20] H. Haberland, M. Moseler, Y. Qiang, O. Rattunde, T. Reiners, Y. Thurner, *Surf. Rev. Lett.* **1996**, *03*, 887.
[21] H. Haberland, in *Gas-Phase Synthesis of Nanoparticles* (Ed: Y. Huttel), Wiley-VCH, Weinheim, Germany **2017**, pp. 1–21.
[22] A. Fischer, R. Kruk, H. Hahn, *Rev. Sci. Instrum.* **2015**, *86*, 023304.
[23] N. Gack, G. Iankevich, C. Benel, R. Kruk, D. Wang, H. Hahn, T. Reisinger, *Nanomaterials* **2020**, *10*, 2192.
[24] C. Benel, T. Reisinger, R. Kruk, H. Hahn, *Adv. Mater.* **2019**, *31*, 1806634.
[25] A. Fischer, R. Kruk, D. Wang, H. Hahn, *Beilstein J. Nanotechnol.* **2015**, *6*, 1158.
[26] E. Jué, G. Iankevich, T. Reisinger, H. Hahn, V. Provenzano, M. R. Pufall, I. W. Haygood, W. H. Rippard, M. L. Schneider, *J. Appl. Phys.* **2022**, *131*, 073902.
[27] H. Natter, M. Schmelzer, R. Hempelmann, *J. Mater. Res.* **1998**, *13*, 1186.
[28] Y. Iguchi, G. L. Katona, C. Cserháti, G. A. Langer, Z. Erdélyi, *Acta Mater.* **2018**, *148*, 49.
[29] F. C. Fonseca, G. F. Goya, R. F. Jardim, R. Muccillo, N. L. V. Carreño, E. Longo, E. R. Leite, *Mater. Res. Soc. Symp. Proc.* **2002**, *746*, 66.
[30] S. Zhu, X. Xiang, X. T. Zu, L. M. Wang, *Nucl. Instrum. Methods Phys. Res. B* **2006**, *242*, 114.
[31] M. A. Turchanin, P. G. Agraval, A. R. Abdulov, *Powder Metall. Met. Ceram.* **2007**, *46*, 467.
[32] X. He, W. Zhong, C.-T. Au, Y. Du, *Nanoscale Res. Lett.* **2013**, *8*, 446.
[33] C. L. Chien, J. Q. Xiao, J. S. Jiang, *J. Appl. Phys.* **1993**, *73*, 5309.
[34] K. D. Bird, M. Schlesinger, *J. Electrochem. Soc.* **1995**, *142*, L65.
[35] V. Vikram, M. R. Rahman, M. Katiyar, *AIP Conf. Proc.* **2008**, *1003*, 37.
[36] E. H. Williams, *Phys. Rev.* **1931**, *38*, 828.
[37] Z. Wang, L. Fang, I. Cotton, R. Freer, *Mater. Sci. Eng., B* **2015**, *198*, 86.
[38] H. Haberland, M. Karrais, M. Mall, *Z. Phys. D: At., Mol. Clusters* **1991**, *20*, 413.
[39] H. Haberland, M. Mall, M. Moseler, Y. Qiang, T. Reiners, Y. Thurner, *J. Vac. Sci. Technol. A* **1994**, *12*, 2925.
[40] K. Thompson, D. Lawrence, D. J. Larson, J. D. Olson, T. F. Kelly, B. Gorman, *Ultramicroscopy* **2007**, *107*, 131.